APC/C^{FZR-1} Controls SAS-5 Levels to Regulate Centrosome Duplication in *Caenorhabditis elegans*

Running title: Centrosome Regulation by the APC/C^{FZR-1}

Jeffrey C. Medley*, Lauren E. DeMeyer*, Megan M. Kabara*, and Mi Hye Song*,†

* Department of Biological Sciences, Oakland University, Rochester, MI 48309, USA.

† To whom correspondence should be addressed.

Contact Information: msong2@oakland.edu

Key words: APC/C; FZR-1; *C. elegans*; Centrosome; E3 ubiquitin ligase; Proteasome; ZYG-1

Abstract

As the primary microtubule-organizing center, centrosomes play a key role in establishing mitotic bipolar spindles that secure correct transmission of genomic content. For the fidelity of cell division, centrosome number must be strictly controlled by duplicating only once per cell cycle. Proper levels of centrosome proteins are shown to be critical for normal centrosome number and function. Overexpressing core centrosome factors leads to extra centrosomes, while depleting these factors results in centrosome duplication failure. In this regard, protein turnover by the ubiquitin-proteasome system provides a vital mechanism for the regulation of centrosome protein levels. Here, we report that FZR-1, the *Caenorhabditis elegans* homolog of Cdh1/Hct1/Fzr, a co-activator of the anaphase promoting complex/cyclosome (APC/C), an E3 ubiquitin ligase, functions as a negative regulator of centrosome duplication in the *Caenorhabditis elegans* embryo. During mitotic cell division in the early embryo, FZR-1 is associated with centrosomes and enriched at nuclei. Loss of *fzr-1* function restores centrosome duplication and embryonic viability to the hypomorphic *zyg-1(it25)* mutant, in part, through elevated levels of SAS-5 at centrosomes. Our data suggest that the APC/C^{FZR-1} regulates SAS-5 levels by directly recognizing the conserved motif, KEN-box, contributing to proper centrosome duplication. Together, our work shows that FZR-1 plays a conserved role in regulating centrosome duplication in *Caenorhabditis elegans.*

Introduction

The centrosome is a small, non-membranous organelle that serves as the primary microtubule-organizing center in animal cells. Each centrosome consists of a pair of barrel-shaped centrioles that are surrounded by a network of proteins called pericentriolar material (PCM). During mitosis, two centrosomes organize bipolar spindles that segregate genomic content equally into two daughter cells. Thus, tight control of centrosome number is vital for the maintenance of genomic integrity during cell division, by restricting centrosome duplication once and only once per cell cycle. Erroneous centrosome duplication results in aberrant centrosome number that leads to chromosome missegregation and abnormal cell proliferation and is associated with human disorders including cancers and microcephaly (Gonczy, 2015; Nigg and Stearns, 2011).

In the nematode *C. elegans,* extensive studies identified a set of core centrosome factors that are absolutely essential for centrosome duplication: the protein kinase ZYG-1 and the coiled-coil proteins SPD2, SAS-4, SAS-5 and SAS-6 (Delattre et al., 2004; Dammerman et al., 2004; Kemp et al., 2004; Kirkham et al., 2003; Leidel et al., 2005; Leidel and Gönczy, 2003; O'Connell et al., 2001; Pelletier et al., 2004). SPD-2 and ZYG-1 localize early to the site of centriole formation and are required for the recruitment of the SAS-5/SAS-6 complex that sequentially recruits SAS-4 to the centriole (Delattre et al., 2006; Pelletier et al., 2006). These key factors are identified in other animal systems, suggesting highly conserved evolutionary mechanisms in centrosome duplication. For instance, the human genome contains homologs of the five centrosome factors found in *C. elegans,* Cep192/SPD-2 (Zhu et al., 2008), Plk4/ZYG-1 (Habedanck et al., 2005), STIL/SAS-5 (Arquint et al., 2012), HsSAS-6/SAS-6 (Leidel et al., 2005) and CPAP/SAS-4 (Kleylein-Sohn et al., 2007; Tang et al., 2009) and all these factors are shown to play a critical role in centrosome biogenesis (Gonczy, 2015; Fu et al., 2015).

Maintaining the proper levels of centrosome proteins is critical for normal centrosome number and function (Brownlee et al., 2011; Holland et al., 2010; Kleylein-Sohn et al., 2007; Levin et al., 2017; Meghini et al., 2016; Puklowski et al., 2011; Rogers et al., 2009; Song et al., 2011; Strnad et al., 2007; Tang et al., 2011). In light of this, protein turnover by proteolysis provides a key mechanism for

regulating the abundance of centrosome factors. A mechanism regulating protein levels is their degradation by the 26S proteasome that catalyzes the proteolysis of poly-ubiquitinated substrates (Livneh et al., 2016). The anaphase promoting complex/cyclosome (APC/C) is a multi-subunit E3 ubiquitin ligase that targets substrates for degradation (Acquaviva and Pines, 2006; Chang and Barford, 2014; Peters, 2006). The substrate specificity of the APC/C is directed through the sequential, cell cycle-dependent activity of two co-activators, Cdc20/Fzy/FZY-1 (Hartwell and Smith, 1985; Dawson et al., 1995; Kitagawa et al., 2002) and Cdh1/Fzr/Hct1/FZR-1 (Sigrist and Lehner, 1997; Schwab et al., 1997; Visintin et al., 1997; Fay et al., 2002). During early mitosis Cdc20 acts as co-activator of the APC/C, and Cdh1 functions as co-activator to modulate the APC/C-dependent events at late mitosis and in G1 (Irniger and Nasmyth, 1997; Visintin et al., 1997; Fang et al., 1998; Prinz et al., 1998; Shirayama et al., 1998). Upregulated targets in Cdh1-deficient cells are shown to be associated with the genomic instability signature of human cancers and show a high correlation with poor prognosis (Carter et al., 2006; Garcia-Higuera et al., 2008). Furthermore, a mutation in SIL/STIL (a human homolog of SAS-5) linked to primary microcephaly (MCPH; Kumar et al., 2009) results in deletion of the Cdh1-dependent destruction motif (KEN-box), leading to deregulated accumulation of STIL protein and centrosome amplification (Arquint et al., 2014). In *Drosophila*, the APC/C$^{Fzr/Cdh1}$ directly interacts with Spd2 through KEN-box recognition and targets Spd2 for degradation (Meghini et al., 2016). Therefore, the APC/C$^{Cdh1/Fzr/Hct1}$ plays a critical role in regulating the levels of key centrosome duplication factors in mammalian cells and flies.

In *C. elegans,* FZR-1 has been shown to be required for fertility, cell cycle progression and cell proliferation during embryonic and postembryonic development via synthetic interaction with *lin-35/Rb* (Fay et al., 2002; The et al., 2016). However, the role of FZR-1 in centrosome assembly has not been described. In this study, we molecularly identified *fzr-1* as a genetic suppressor of *zyg-1.* Our results suggest that APC/C^{FZR-1} negatively regulates centrosome duplication, in part, through proteasomal degradation of SAS-5 in a KEN-box dependent fashion. Therefore, FZR-1, the *C. elegans* homolog of Cdh1/Hct1/Fzr, plays a conserved role in centrosome duplication.

Materials and Methods

C. elegans strains and genetics

A full list of *C. elegans* strains used in this study is listed in Table S1. All strains were derived from the wild-type Bristol N2 strain using standard genetic methods (Brenner et al., 1974, Church et al., 1995). Strains were maintained on MYOB plates seeded with *E. coli* OP50 and grown at 19° unless otherwise indicated. The *fzr-1::gfp::3xflag* construct containing 21.6Kbp of the *fzr-1* 5'UTR and 6Kbp of the *fzr-1* 3'UTR was acquired from TransgenOme (construct number: 7127141463160758 F11, Sarov et al., 2012), which was used to generate the transgenic line, MTU10, expressing C-terminal GFP-tagged FZR-1. For the generation of N-terminal GFP-tagged FZR-1 (OC190), we used Gateway cloning (Invitrogen, Carlsbad, CA, USA) to generate the construct. Coding sequence of *fzr-1* was PCR amplified from the cDNA clone yk1338f2, and cloned into pDONR221 (Invitrogen) and then the resulting pDONR construct was recombined into pID3.01 (pMS9.3), which is driven by the *pie-1* promotor. The transgenes were introduced into worms by standard particle bombardment (Praitis et al., 2001). For embryonic viability and brood size assays, individual L4 animals were transferred to clean plates and allowed to self-fertilize for 24 hours at the temperatures indicated. For brood size assays, this was repeated until animals no longer produced fertilized embryos. Progeny were allowed at least 24 hours to complete embryogenesis before counting the number of progeny. The *fzr-1(RNAi)* experiments were performed by RNAi soaking (Song et al., 2008). To produce dsRNA for RNAi soaking, we amplified a DNA template from the cDNA clone yk1338f2 using the primers 5'-ATGGATGAGCAACCGCC-3' and 5'-GCACTGTACGTAAAAAGTGATC-3' that contained a T7 promoter sequence at their 5' ends. *In vitro* transcription was performed using the T7-MEGAscript kit (Thermo-Fisher, Hanover park, IL, USA). L4 animals were soaked overnight in M9 buffer containing either 0.1-0.4 mg dsRNA/mL or no dsRNA (control).

Mapping and molecular identification of *szy-14*

We mated *zyg-1(it25) dpy-10(e128) szy-14(bs31) unc-4(e120)* hermaphrodites with Hawaiian, CB4856 males for single-nucleotide polymorphism mapping (Song et al., 2008), and isolated a total of 104 independent Dpy-nonUnc from the F2 generation. After established homozygous recombinant lines, we scored for the presence of *szy-14(bs31)* based on the suppression of the *zyg-1(it25)* mutant (additionally, reduced brood size; Fay et al., 2002). In parallel, we used *zyg-1(it25), zyg-1(it25) dpy-10(e128), zyg-1(it25) dpy-10(e128) szy-14(bs31) unc-4(e120), zyg-1(it25) szy-14(bs31),* and *zyg-1(it25) szy-14(bs31) unc-4(e120)* as controls. For the molecular identification of the mutation, we sequenced several candidate genes (*nos-3, kin-15, kin-16, wee-1.1, wee-1.3,* and *fzr-1*) located within an interval on chromosome II. For sequencing the *fzr-1* gene, we used the following primers: Forward 5'-TCTTGTTTCTGGTGGAGGT-3' and Reverse 5'- ACACGATACTGATGCCCAA-3' for the *bs31* suppressor, and Forward 5'- ATGGATGAGCAGCAACCGCC-3' and Reverse 5'-CAAGCTTGAGCTGTTGG-3' for the *bs38* suppressor. Purified PCR amplicons were sequenced and aligned to the ORF, ZK1307.6 to identify the nucleotide substitution.

CRISPR/CAS-9 mediated genome editing

For genome editing, we used the co-CRISPR technique as previously described in *C. elegans* (Arribere et al.., 2014; Paix et al., 2015). In brief, we microinjected N2 and *zyg-1(it25)* animals using mixture containing recombinant SpCas9 (Paix et al., 2015), crRNAs targeting *sas-5* and *dpy-10* at 0.4-0.8μg/μL, tracrRNA at 12μg/μL, and single-stranded DNA oligonucleotides to repair *sas-5* and *dpy-10* at 25-100ng/μL. Microinjection was performed using the XenoWorks microinjector (Sutter Instruments, Novato, CA, USA) with a continuous pulse setting at 400-800 hPa. All RNA and DNA oligonucleotides used in this study were synthesized by Integrated DNA Technologies (IDT, Coralville, IA, USA) and are listed in Table S2. As we were unable to engineer a silent mutation into the PAM sequence used by the *sas-5* crRNA, we introduced six silent mutations to *sas-5* (aa 201-206) by mutating 8 out of 20 the nucleotides that comprise the *sas-5* crRNA, in order to disrupt Cas9 recognition after homology-directed repair. After injection, animals were allowed to produce F1 progeny that were monitored for the presence of *dpy-10(cn64)/+* rollers. To identify the *sas-5*$^{KEN\text{-}to\text{-}3A}$ mutation, we extracted genomic DNA

from broods containing the highest frequency of F1 rollers. Using the primers, forward: 5'-TGCCCAAAATACGACAACG-3' and reverse: 5'-TACACTACTCACGTCTGCT-3', we amplified the region of *sas-5* containing the KEN-box sequence. As the repair template for the *sas-5*$^{KEN\text{-}to\text{-}3A}$ mutation introduces an Hpy8I restriction enzyme (NEB, Ipswich, MA, USA) cutting site, we used an Hpy8I enzyme digestion to test for the introduction of our targeted mutation. After isolating homozygotes based on the Hpy8I cutting, we confirmed the *SAS-5*$^{KEN\text{-}to\text{-}3A}$ mutation by genomic DNA sequencing. Sequencing revealed that several lines were homozygous for the *SAS-5*$^{KEN\text{-}to\text{-}3A}$ mutation (Table S1, Figure 5A). However, the strain MTU14, contained the entire silent mutations that we designed to disrupt Cas9 recognition without affecting KEN-box (Table S1, Figure 5A). Thus, we used MTU14 as a control for our assays.

Cytological analysis

To perform immunostaining, the following antibodies were used at 1:2,000-3,000 dilutions: α-Tubulin (DM1a; Sigma, St-Louis, MO, USA), α-GFP: IgG$_1$κ (Roche, Indianapolis, IN, USA), α-ZYG-1 (Stubenvoll et al., 2016), α-TBG-1 (Stubenvoll et al., 2016), α-SAS-4 (Song et al., 2008), α-SAS-5 (Medley et al., 2017), and Alexa Fluor 488 and 561 (Invitrogen, Carlsbad, CA, USA) as secondary antibodies. Confocal microscopy was performed as described (Stubenvoll et al., 2016) using a Nikon Eclipse Ti-U microscope equipped with a Plan Apo 60 x 1.4 NA lens, a Spinning Disk Confocal (CSU X1) and a Photometrics Evolve 512 camera. Images were acquired using MetaMorph software (Molecular Devices, Sunnyvale, CA, USA). MetaMorph was used to draw and quantify regions of fluorescence intensity and Adobe Photoshop CS6 was used for image processing. To quantify centrosomal SAS-5 signals, the average intensity within an 8-pixel (1 pixel = 0.151 μm) diameter region was measured within an area centered on the centrosome and the focal plane with the highest average intensity was recorded. Centrosomal TBG-1 (γ-tubulin) levels were quantified in the same manner, except that a 25-pixel diameter region was used. For both SAS-5 and TBG-1 quantification, the average fluorescence intensity within a 25-pixel diameter region drawn outside of the embryo was used for background subtraction.

Immunoprecipitation (IP)

Embryos were collected from gravid worms using hypochlorite treatment (1:2:1 ratio of M9 buffer, 5.25% sodium hypochlorite and 5M NaCl), washed with M9 buffer five times and frozen in liquid nitrogen. Embryos were stored at -80° until use. IP experiment using α-GFP were performed following the protocol described previously (Stubenvoll et al., 2016). 20 µL of Mouse-α-GFP magnetic beads (MBL, Naka-ku, Nagoya, Japan) were used per reaction. The α-GFP beads were prepared by washing twice for 15 minutes in PBST (PBS; 0.1% Triton-X), followed by a third wash in 1x lysis buffer (50 mM HEPES [pH 7.4], 1mM EDTA, 1mM $MgCl_2$, 200 mM KCl, and 10% glycerol (v/v)) (Cheeseman et al., 2004). Embryos were suspended in 1 x lysis buffer supplemented with complete protease inhibitor cocktail (Roche, Indianapolis, IN, USA) and MG132 (Tocris, Avonmouth, Bristol, UK). The embryos were then milled for three minutes at 30 Hz using a Retsch MM 400 mixer-mill (Verder Scientific, Newtown, PA, USA). Lysates were sonicated for three minutes in ice water using an ultrasonic bath (Thermo-Fisher, Hanover Park, IL, USA). Samples were spun at 45,000RPM for 45 minutes using a Sorvall RC M120EX ultracentrifuge (Thermo-Fisher, Hanover Park, IL, USA). The supernatant was transferred to clean microcentrifuge tubes. Protein concentration was quantified using a NanoDrop spectrophotometer (Thermo-Fisher, Hanover Park, IL, USA) and equivalent amount of total proteins was used for each reaction. Samples and α-GFP beads were incubated and rotated for one hour at 4ºC and then washed five times for five minutes using PBST (PBS + 0.1% Triton-X 100). Samples were resuspended in 20 µL of a solution containing 2X Laemmli Sample Buffer (Sigma, St-Louis, MO, USA) and 10% β-mercaptoethanol (v/v), then boiled for five minutes. For protein input, 5 µL of embryonic lysates were diluted using 15 µL of a solution containing 2X Laemmli Sample Buffer and 10% β-mercaptoethanol (v/v) and boiled for 5 minutes before fractionating on a 4-12% NuPAGE Bis-Tris gel (Invitrogen, Carlsbad, CA, USA).

Western Blotting

For western blotting, samples were sonicated for five minutes and boiled in a solution of 2X Laemmli Sample Buffer and 10% β-mercaptoethanol before being fractionated on a 4-12% NuPAGE Bis-Tris gel (Invitrogen, Carlsbad, CA, USA). The iBlot Gel Transfer system (Invitrogen, Carlsbad, CA, USA) was then used to transfer samples to a nitrocellulose membrane. The following antibodies were used at 1:3,000-10,000 dilutions: α-Tubulin: α-Tubulin (DM1a; Sigma, St-Louis, MO, USA), α-GFP: $IgG_1κ$ (Roche, Indianapolis, IN, USA), α-SAS-5 (Song et al., 2011) and α-TBG-1 (Stubenvoll et al., 2016). IRDye secondary antibodies (LI-COR Biosciences, Lincoln, NE, USA) were used at a 1:10,000 dilution. Blots were imaged using the Odyssey infrared scanner (LI-COR Biosciences, Lincoln, NE, USA), and analyzed using Image Studio software (LI-COR Biosciences, Lincoln, NE, USA).

Statistical Analysis

All *p*-values were calculated using two-tailed t-tests assuming equal variance among sample groups. Statistics are presented as Average ± standard deviation (SD) unless otherwise specified. Data were independently replicated at least three times for all experiments and subsequently analyzed for statistical significance.

Data Availability

All strains used in this study are available upon request. The following supplemental materials are uploaded.

Figure S1. Centrosome-associated TBG-1 levels are unaffected in *fzr-1(bs31)* and *sas-5*$^{KEN\text{-}to\text{-}3A}$ mutant embryos.

Figure S2. Brood size in *sas-5*$^{KEN\text{-}to\text{-}3A}$ and *fzr-1(bs31)* mutants.

Figure S3. SAS-5 levels are increased in *sas-5*$^{KEN\text{-}to\text{-}3A}$ mutants.

Table S1. List of strains used in this study.

Table S2. List of oligonucleotides used for CRISPR/Cas9 genome editing.

Results and Discussion

The *szy-14* mutation restores centrosome duplication to *zyg-1(it25)* mutants

Through a genetic suppressor screen (Kemp et al., 2007), the *szy-14* (suppressor of *zyg-1*) gene was originally identified that restores embryonic viability of the partial loss-of-function *zyg-1(it25)* mutant. The *zyg-1(it25)* mutant embryo grown at the restrictive temperature (24°) fails to duplicate centrosomes during the first cell cycle, resulting in monopolar spindles at the second mitosis and 100% embryonic lethality (O'Connell et al., 2001). Complementation test identified two alleles, *szy-14(bs31)* and *szy-14(bs38)*, of the *szy-14* mutation that partially restore the embryonic viability of *zyg-1(it25)* but show no obvious cytological defects but slow growth phenotype, indicating that the *szy-14* gene is not essential for embryonic viability (Table 1, Kemp et al., 2007).

Given that ZYG-1 is essential for proper centrosome duplication (O'Connell et al., 2001), we speculated that the *szy-14* mutation might suppress the embryonic lethality of *zyg-1(it25)* mutants via restoration of centrosome duplication. To examine centrosome duplication events, we quantified the percentage of bipolar spindles at the second mitosis, which indicates successful centrosome duplication during the first cell cycle (Figure 1A and B). At the restrictive temperature 24°, both double mutant embryos, *zyg-1(it25); szy-14(bs31)* (79.9±22.0%) and *zyg-1(it25); szy-14(bs38)* (51.4±24.4%) produced bipolar spindles at a significantly higher rate, compared to *zyg-1(it25)* single mutant embryos (3.3±4.4%) (Figure 1B). Our observation suggests that the *szy-14* mutation restores centrosome duplication in *zyg-1(it25)* embryos, thereby restoring embryonic viability to *zyg-1(it25)* mutants.

Molecular identification of *szy-14*

The *szy-14* gene was initially mapped to the right arm of chromosome II between the morphological markers *dpy-10* and *unc-4* (Kemp et al., 2007). Using fine physical mapping, we located *szy-14* to an interval of 161-Kb (ChrII: 9621265..9782352; Wormbase.org) that contains several known cell cycle regulators. Based on the genetic map position of the *szy-14* suppressor, we have sequenced candidate genes within this interval to detect any mutations in *szy-14* mutants. Sequencing the *fzr-1* genome

region revealed that *szy-14(bs38)* mutants contain a single substitution (C-to-T) in exon 2, and *szy-14(bs31)* mutants carry a mutation (G-to-A) in exon 5 of the ORF ZK1307.6 that corresponds to the *fzr-1* gene. Consistently, inhibiting FZR-1 by RNAi soaking partially restores embryonic viability in both *zyg-1(it25)* and *zyg-1(or409)* mutant alleles (Table 1), indicating that loss-of-function of *fzr-1* leads to the restoration of embryonic viability to the *zyg-1* mutants. Together, we determined that the *bs31* and *bs38* mutations are alleles of the *fzr-1* gene. Hereafter, we refer to *szy-14(bs31)* and *szy-14(bs38)* mutants as *fzr-1(bs31)* and *fzr-1(bs38)* mutants, respectively.

fzr-1 encodes a conserved co-activator of the anaphase promoting complex/cyclosome (APC/C), the *C. elegans* homolog of Cdh1/Hct1/Fzr (Fay et al., 2002; Schwab et al., 1997; Sigrist and Lehner, 1997; Visintin et al., 1997). The APC/C is an E3 ubiquitin ligase that orchestrates the sequential degradation of key cell cycle regulators during mitosis and early interphase (Song and Rape, 2008). As part of this process, specific activators modulate the APC/C activity in different phases of mitosis. Specifically, FZR-1/Cdh1 modulates the APC/C at late mitosis and events in G1 during the time when centrosome duplication occurs. In each of the *fzr-1* mutant alleles, the single substitution leads to a missense mutation (Figure 1C). The *fzr-1(bs31)* mutation results in a missense mutation (C612Y) within the conserved WD40-repeat domain that is known to be involved in protein-protein interactions and is important for substrate recognition (Kraft et al., 2005; He et al., 2013). The *fzr-1(bs38)* mutation produces a missense mutation (R65C) at the conserved C-box of FZR-1. The C-box is known to be crucial for the physical interaction between FZR-1 and other APC/C subunits (Schwab et al., 2001; Thornton et al., 2006; Chang et al., 2015; Zhang et al., 2016). Thus, both *fzr-1(bs31)* and *fzr-1(bs38)* mutations appear to affect conserved domains that are known to be critical for the function of the APC/C complex, suggesting that FZR-1 might regulate centrosome duplication through the APC/C complex.

FZR-1 localizes to nuclei and centrosomes during early cell division

To determine where FZR-1 might function during the early cell cycle, we produced two independent transgenic strains that express FZR-1 tagged with GFP at the N- or C-terminus (see method and

materials). To label microtubules, we mated GFP-tagged FZR-1 transgenic animals with the mCherry::β-tubulin expressing line, and performed 4D time-lapse movies to observe subcellular localization of FZR-1 throughout the first cell cycle (Figure 2A). Confocal imaging illustrates that during interphase and early mitosis, FZR-1 is highly enriched at the nuclei. After the nuclear envelope breaks down (NEBD), FZR-1 diffuses to the cytoplasm and reappears to the nuclei at late mitosis when the nuclear envelop reforms. After NEBD, FZR-1 becomes apparent at spindle microtubules, and centrosomes that co-localize with SPD-2, a centrosome protein (Figure 2B). Both GFP-tagged FZR-1 transgenic embryos exhibit similar subcellular distributions, except a slight difference in fluorescent intensity. Our observations suggest that *C. elegans* FZR-1 might direct APC/C activity at centrosomes during late mitosis in early embryos, which is consistent with the role of FZR-1 as the co-activator of the APC/C at late mitosis in other organisms (Meghini et al., 2016; Raff et al., 2002; Zhou et al., 2003).

FZR-1 might function as a part of the APC/C complex to regulate centrosome duplication

Given that FZR-1 is a conserved co-activator of the APC/C, an E3 ubiquitin ligase, we hypothesized that FZR-1 functions as a part of the APC/C complex in centrosome assembly. If so, depleting other APC/C subunits should have a similar effect that loss of FZR-1 had on the *zyg-1(it25)* mutant. To examine how other core subunits of the APC/C complex might affect *zyg-1(it25)* mutants, we mated the *zyg-1(it25)* strain with *mat-3(or180)* mutants for the core APC8/CDC23 subunit (Golden et al., 2000), and *emb-1(hc57)* mutants for the conserved subunit APC16 in the *C. elegans* APC/C complex (Greens et al., 2011; Kops et al., 2011; Shakes et al., 2011). By generating double homozygote mutants, we assayed for bipolar spindle formation and embryonic viability in *zyg-1(it25); mat-3(or180)* and *zyg-1(it25); emb-1(hc57)* double homozygous mutants (Figure 3, Table 1). At the restrictive temperature 24°, *zyg-1(it25); mat-3(or180)* double mutant embryos exhibit a 9-fold increase in bipolar spindle formation (81.8±14.3%), compared to *zyg-1(it25)* single mutant embryos (9.1±8.8%) during the second mitosis (Figure 3A). Consistently, 5% of *zyg-1(it25); mat-3(or180)* double mutants produce viable progeny while 100% of *zyg-1(it25)* or *mat-3(or180)* single mutant progeny die at 24° (Table 1). In support of our results, the *mat-3(bs29)* allele has been reported as a genetic suppressor of *zyg-1* (Miller

et al., 2016). Furthermore, we observed that the *emb-1* mutation suppresses the centrosome duplication phenotype of *zyg-1(it25)* mutants at the semi-restrictive temperature 22.5°. While 45.5±11.9% of *zyg-1(it25)* embryos form bipolar spindles, 79.1±12.4% of *zyg-1(it25); emb-1(hc57)* double mutant embryos produce bipolar spindles (Figure 3A). We, however, observed no significant restoration of embryonic viability in *zyg-1(it25); emb-1(hc57)* double mutants (p=0.691) compared to *zyg-1(it25)* single mutants (Table 1), presumably due to the strong embryonic lethality by the *emb-1(hc57)* mutation itself (Kops et al., 2011; Shakes et al., 2011). Our results indicate that the APC/C complex functions to suppress the phenotype of *zyg-1(it25)* mutants. Therefore, FZR-1 might function as a component of the APC/C complex to regulate centrosome duplication in early *C. elegans* embryos.

Loss of FZR-1 results in elevated SAS-5 levels

Next we wanted to understand how FZR-1 contributes to centrosome duplication. Since FZR-1 appears to function through the APC/C complex in centrosome assembly, we hypothesized that the APC/C^{FZR-1} specifically targets one or more centrosome regulators for ubiquitin-mediated degradation. If that is the case, depleting FZR-1 should protect substrates from degradation leading to accumulation of target proteins. To identify a direct substrate of APC/C^{FZR-1} that regulates centrosome assembly, we utilized the conserved FZR-1 co-activator specific recognition motif, KEN-box, to screen for a potential substrate (Pfleger and Kirschner, 2000). The KEN-box appears to be the major degron motif that APC/C^{FZR-1} recognizes in centrosome duplication (Arquint et al., 2014; Meghini et al., 2016; Strnad et al., 2007; Tang et al., 2009). In human cells, HsSAS-6, STIL/SAS-5, and CPAP/SAS-4 contain KEN-box motif, and APC/C$^{Cdh1/FZR-1}$ targets these proteins for ubiquitin-mediated proteolysis, thereby preventing extra centrosomes (Arquint et al., 2014; Strnad et al., 2007; Tang et al., 2009). The *Drosophila* APC/C$^{Fzr/Cdh1/FZR-1}$ is also shown to target Spd2 for destruction through a direct interaction with KEN-box (Meghini et al., 2016). Interestingly, *C. elegans* SAS-4 and SAS-6 lack a KEN-box. Instead, SAS-5 contains a KEN-box indicating an evolutionary divergence between humans and nematodes.

Protein stabilization by the *fzr-1* mutation might lead to increased levels of a centrosome-associated substrate, which may compensate for impaired ZYG-1 function at the centrosome. In *C. elegans,* SAS-5 is the only core centrosome duplication factor containing a KEN-box, which suggests SAS-5 as a potential target of the APC/C^{FZR-1}. If the APC/C^{FZR-1} targets SAS-5 directly through KEN-box for ubiquitin-mediated proteolysis, inhibiting FZR-1 should protect SAS-5 from degradation leading to SAS-5 accumulation. To examine how the *fzr-1* mutation affected SAS-5 stability, we immunostained embryos with anti-SAS-5, and quantified the fluorescence intensity of centrosome-associated SAS-5 (Figure 4A and 4B). As ZYG-1 is required for SAS-5 localization to centrosomes, hyper-accumulation of SAS-5 might compensate for partial loss-of-function of ZYG-1, thereby restoring centrosome duplication to *zyg-1(it25)* mutants. In fact, our quantitative immunofluorescence revealed that *fzr-1(bs31)* embryos exhibit a significant increase (1.41±0.42 fold; $p<0.001$) in centrosomal SAS-5 levels at the first anaphase, compared to wild-type (Figure 4B). Consistently, compared to *zyg-1(it25)* single mutants, *zyg-1(it25); fzr-1(bs31)* double mutant embryos exhibit a 1.48-fold increase ($p<0.001$) in centrosome-associated SAS-5 levels (Figure 4B). Indeed, centrosomal SAS-5 are restored to near wild-type levels in *zyg-1(it25); fzr-1(bs31)* double mutants (0.95±0.44 fold; $p=0.003$). However, we observed no significant changes in centrosomal TBG-1 (γ-tubulin) levels in *fzr-1(bs31)* mutants (Figure S1).

Elevated protein levels might influence centrosome-associated SAS-5 levels in *fzr-1(bs31)* mutants. To determine how inhibition of the APC/C^{FZR-1} affected overall protein levels, we performed quantitative western blot analysis using embryonic protein lysates and antibodies against centrosome proteins (Figure 4C). Our data indicate that *fzr-1(bs31)* embryos possess increased SAS-5 levels (~1.5-fold), relative to wild-type embryos, while the levels of SAS-6 and TBG-1 appear to be unaffected in *fzr-1(bs31)* mutants (Figure 4C). Our observation in SAS-6 levels in *fzr-1(bs31)* mutants is consistent with previous work by Miller et al., 2016, showing no increase in SAS-6 levels by the *mat-3(bs29)*/APC8 mutation that inhibits the APC/C function. These results suggest that *C. elegans* utilizes a different mechanism to control SAS-6 levels, unlike Human SAS-6 that is regulated by the APC/C-mediated proteolysis (Strnad et al., 2007). Furthermore, our immunoprecipitation suggests a physical interaction between SAS-5 and FZR-1 in *C. elegans* embryos (Figure 4D), supporting that SAS-5 might be a direct

substrate of the APC/C^{FZR-1}. Consistent with our results in this study, prior study has shown that inhibiting the 26S proteasome leads to increased levels of SAS-5 (Song et al., 2011). Thus, SAS-5 levels are likely to be controlled through the ubiquitin-proteasome system.

Together, our data show that the *fzr-1* mutation leads to a significant increase in both cellular and centrosomal levels of SAS-5, suggesting that the APC/C^{FZR-1} might control SAS-5 levels via ubiquitin-mediated proteasomal degradation to regulate centrosome assembly in the *C. elegans* embryo.

Mutation of KEN-box stabilizes SAS-5

If the APC/C^{FZR-1} directly targets substrates for destruction via the conserved KEN-box, mutating this motif should cause substantial resistance to the ubiquitination-mediated degradation. To determine whether the APC/C^{FZR-1} targets SAS-5 through the KEN-box motif, we mutated the KEN-box at the endogenous *sas-5* locus. By using CRISPR/CAS-9 mediated genome editing (Paix et al., 2015), we generated mutant lines (*sas-5*$^{KEN-to-3A}$) carrying alanine substitutions of the SAS-5 KEN-box (Figure 5A). The *sas-5*$^{KEN-to-3A}$ mutant embryo exhibits no obvious cell cycle defects or embryonic lethality (Table 1), consistent with *fzr-1* mutants (Kemp et al., 2007). *sas-5*$^{KEN-to-3A}$ animals exhibit a slightly reduced (~80%) and irregular distribution of brood size within the population (Figure S2). Reduced brood size and slow growth phenotypes were previously reported in *fzr-1* mutant alleles (Fay et al., 2002; Kemp et al., 2007).

Next, we asked how the *sas-5*$^{KEN-to-3A}$ mutation affected *zyg-1(it25)* mutants. If the APC/C^{FZR-1}-mediated proteolysis of SAS-5 accounts for the suppression of *zyg-1, sas-5*$^{KEN-to-3A}$ mutants should mimic the *fzr-1* mutation that suppresses *zyg-1* mutants. By mating the *sas-5*$^{KEN-to-3A}$ mutant with *zyg-1(it25)* animals, we tested whether the *sas-5*$^{KEN-to-3A}$ mutation could genetically suppress *zyg-1* mutants, by assaying for embryonic viability and centrosome duplication (Table 1, Figure 5B). For the *zyg-1(it25)* mutant control in this experiment, we used the strain MTU14 [*zyg-1(it25); sas-5*$^{KEN-to-KEN}$, Table S1] that contains the equivalent modifications, except KEN-box, to the *sas-5*$^{KEN-to-3A}$ mutation (Figure 5A, see methods and materials). At the semi-restrictive temperature 22.5°, *zyg-1(it25)*; *sas-5*$^{KEN-to-3A}$ animals

lead to a 7.7-fold increase in the frequency of viable progeny (35.3±9.2%; p<0.0001), compared to *zyg-1(it25); sas-5*$^{KEN\text{-}to\text{-}KEN}$ mutant controls (4.6±4.0%) (Table 1). Consistently, *zyg-1(it25)*; *sas-5*$^{KEN\text{-}to\text{-}3A}$ embryos exhibit successful bipolar spindle assembly at a significantly higher rate (67.5±16.3%; p=0.02) than *zyg-1(it25); sas-5*$^{KEN\text{-}to\text{-}KEN}$ embryos (35.1±10.7%) at the two-cell stage (Figure 5B). These results suggest that the *sas-5*$^{KEN\text{-}to\text{-}3A}$ mutation does partially restore embryonic viability and centrosome duplication to *zyg-1(it25)* mutants at 22.5°. However, at the restrictive temperature 24° where the *fzr-1* mutation shows a strong suppression (Table1, Figure 1B), both *zyg-1(it25)*; *sas-5*$^{KEN\text{-}to\text{-}3A}$ double mutants and *zyg-1(it25); sas-5*$^{KEN\text{-}to\text{-}KEN}$ mutant animals result in 100% embryonic lethality (Table 1). *zyg-1(it25)*; *sas-5*$^{KEN\text{-}to\text{-}3A}$ embryos (bipolar: 14.7%, n=68) grown at 24° show only minor effect on centrosome duplication compared to *zyg-1(it25); sas-5*$^{KEN\text{-}to\text{-}KEN}$ control embryos (bipolar: 7.6%, n=66). The data obtained at 24° reveal that the *sas-5*$^{KEN\text{-}to\text{-}3A}$ mutation leads to much weaker suppression of *zyg-1(it25)* mutants than the *fzr-1* mutation, suggesting that the SAS-5 KEN-box mutation cannot generate the equivalent impact that results from the *fzr-1* mutation. If SAS-5 is the only APC/C$^{FZR\text{-}1}$ substrate that contributes to the suppression of *zyg-1* mutants, the *fzr-1* or KEN-box mutation might influence SAS-5 stability differently. In this scenario, FZR-1 might target SAS-5 through KEN-box and additional recognition motifs (e.g., D-box), causing a greater effect on SAS-5 stability than the KEN-box mutation alone. To examine SAS-5 levels in *sas-5*$^{KEN\text{-}to\text{-}3A}$ mutants, we measured the fluorescence intensity of SAS-5 at centrosomes by quantitative immunofluorescence (Figure 5C and 5D). At 22.5° where the *sas-5*$^{KEN\text{-}to\text{-}3A}$ mutation restores centrosome duplication and embryonic viability to *zyg-1(it25)*, *sas-5*$^{KEN\text{-}to\text{-}3A}$ mutants exhibit a significant increase in centrosome-associated SAS-5 levels (~1.5-fold, p=0.0004), compared to wild-type (Figure 5C and D). Consistently, *zyg-1(it25)*; *sas-5*$^{KEN\text{-}to\text{-}3A}$ embryos display ~1.4-fold (p=0.002) increased SAS-5 levels at centrosomes, compared to *zyg-1(it25); sas-5*$^{KEN\text{-}to\text{-}KEN}$ control embryos that contain reduced centrosomal SAS-5 levels (Figure 5D). Notably, *zyg-1(it25)*; *sas-5*$^{KEN\text{-}to\text{-}3A}$ embryos exhibit centrosomal SAS-5 levels nearly equivalent (~0.97 fold) to those of wild-type embryos (Figure 5D). As a control, we also quantified centrosomal TBG-1 levels but saw no changes between *sas-5*$^{KEN\text{-}to\text{-}3A}$ mutants and the wild-type (Figure S1). Furthermore, we examined overall SAS-5 levels by quantitative western blot, finding that relative to wild-type embryos, *sas-5*$^{KEN\text{-}to\text{-}3A}$

mutant embryos possess ~1.5-fold increased SAS-5 levels (Figure S3). Together, our quantification data reveal that the *sas-5*$^{KEN\text{-}to\text{-}3A}$ or *fzr*-1 mutation leads to nearly equivalent fold change (~1.5-fold) in both cellular and centrosome-associated SAS-5 levels (Figure 4B, 4C, 5D and S3). Together, these results suggest that APC/C$^{FZR\text{-}1}$ directly targets SAS-5 in a KEN-box dependent manner to control SAS-5 turnover, and that SAS-5 stabilization by blocking proteolysis results in elevated SAS-5 levels at the centrosome, contributing to the suppression of the *zyg-1(it25)* mutation.

Interestingly, although either inhibiting FZR-1 or mutating KEN-box influences SAS-5 stability at the comparable level, we observe a notable difference in the suppression level by these two mutations. Weaker suppression by the *sas*-5$^{EN\text{-}to\text{-}3A}$ mutation suggests that the APC/C$^{FZR\text{-}1}$ might target additional substrates that cooperatively support the *zyg*-1 suppression. In this scenario, APC/C$^{FZR\text{-}1}$ might target other centrosome proteins outside core duplication factors through the conserved degron motifs. Alternatively, APC/C$^{FZR\text{-}1}$ targets additional core centrosome factors through other recognition motifs other than KEN-box, such as destruction (D)-box (Glotzer et al., 1991) or unknown motif in the *C. elegans* system. In humans and flies, APC/C$^{Cdh1/Fzr}$ has been shown to regulate the levels of STIL/SAS-5, Spd2, HsSAS-6 and CPAP/SAS-4 (Arquint et al., 2012; Meghini et al., 2016; Strnad et al., 2007; Tang et al., 2009). While *C. elegans* homologs of these factors, except SAS-5, lack KEN-box, all five centrosome proteins contain at least one putative D-box. An intriguing possibility, given the strong genetic interaction observed between *fzr-1* and *zyg-1,* is that ZYG-1 could be a novel substrate of APC/C$^{FZR\text{-}1}$. Additional work will be required to understand the complete mechanism of APC/C$^{FZR\text{-}1}$-dependent regulation of centrosome duplication in *C. elegans*.

In human cells, APC/C^{Cdh1} recognizes a KEN-box to regulate the levels of STIL, the homolog of *C. elegans* SAS-5, and STIL depleted of KEN-box leads to accumulation of STIL protein, and centrosome amplification (Arquint et al., 2014). While we observe no extra centrosomes by the SAS-5 KEN-box mutation, our data show that that APC/C$^{FZR\text{-}1}$ controls SAS-5 stability via the direct recognition of the conserved degron motif, KEN-box, to regulate centrosome duplication in *C. elegans* embryos, suggesting a conserved mechanism for regulating SAS-5 levels between humans and nematodes.

Acknowledgements

We thank members of Song lab (Naomi Haque, Brittany Rettig and Michael Stubenvoll) for their technical support, Kevin O'Connell and Andy Golden for RNAi and worm stains. We especially thank WormBase and the *Caenorhabditis* Genetics Center (CGC). WormBase is supported by grant U41 HG002223 from the National Human Genome Research Institute at the US National Institutes of Health, the UK Medical Research Council and the UK Biotechnology and Biological Sciences Research Council. The CGC (St. Paul, MN), is funded by the National Institutes of Health Office of Research Infrastructure Programs (P40 OD010440).

Competing Interests

No competing interests declared.

Author Contributions

J.C.M. and M.H.S. designed the experiments and wrote the manuscript. J.C.M. and M.H.S. performed quantifications of confocal imaging and protein levels from western blots. J.C.M., L.E.D. M.M.K., and M.H.S. performed experiments and provided data.

Funding

This work was supported by a grant [7R15GM11016-02 to M.H.S.] from the National Institute of General Medical Sciences, and Research Excellence Fund (to M.H.S) from the Center for Biomedical Research at Oakland University. The funders had no role in study design, data collection and analysis, decision to publish, or preparation of the manuscript.

References

Acquaviva, C., and J. Pines, 2006 The anaphase-promoting complex/cyclosome: APC/C. J Cell Sci 119**:** 2401-2404.

Arquint, C., and E. A. Nigg, 2014 STIL microcephaly mutations interfere with APC/C-mediated degradation and cause centriole amplification. Curr Biol 24**:** 351-360.

Arquint, C., K. F. Sonnen, Y. D. Stierhof and E. A. Nigg, 2012 Cell-cycle-regulated expression of STIL controls centriole number in human cells. J Cell Sci 125**:** 1342-1352.

Arribere, J. A., R. T. Bell, B. X. Fu, K. L. Artiles, P. S. Hartman *et al.*, 2014 Efficient marker-free recovery of custom genetic modifications with CRISPR/Cas9 in Caenorhabditis elegans. Genetics 198**:** 837-846.

Brenner, S., 1974 The genetics of Caenorhabditis elegans. Genetics 77**:** 71-94.

Brownlee, C. W., J. E. Klebba, D. W. Buster and G. C. Rogers, 2011 The Protein Phosphatase 2A regulatory subunit Twins stabilizes Plk4 to induce centriole amplification. J Cell Biol 195**:** 231-243.

Carter, S. L., A. C. Eklund, I. S. Kohane, L. N. Harris and Z. Szallasi, 2006 A signature of chromosomal instability inferred from gene expression profiles predicts clinical outcome in multiple human cancers. Nat Genet 38**:** 1043-1048.

Chang, L., and D. Barford, 2014 Insights into the anaphase-promoting complex: a molecular machine that regulates mitosis. Curr Opin Struct Biol 29**:** 1-9.

Chang, L., Z. Zhang, J. Yang, S. H. McLaughlin and D. Barford, 2015 Atomic structure of the APC/C and its mechanism of protein ubiquitination. Nature 522**:** 450-454.

Cheeseman, I. M., S. Niessen, S. Anderson, F. Hyndman, J. R. Yates, 3rd *et al.*, 2004 A conserved protein network controls assembly of the outer kinetochore and its ability to sustain tension. Genes Dev 18**:** 2255-2268.

Church, D. L., K. L. Guan and E. J. Lambie, 1995 Three genes of the MAP kinase cascade, mek-2, mpk-1/sur-1 and let-60 ras, are required for meiotic cell cycle progression in Caenorhabditis elegans. Development 121**:** 2525-2535.

Dammermann, A., T. Muller-Reichert, L. Pelletier, B. Habermann, A. Desai *et al.*, 2004 Centriole assembly requires both centriolar and pericentriolar material proteins. Dev Cell 7**:** 815-829.

Dawson, I. A., S. Roth and S. Artavanis-Tsakonas, 1995 The Drosophila cell cycle gene fizzy is required for normal degradation of cyclins A and B during mitosis and has homology to the CDC20 gene of Saccharomyces cerevisiae. J Cell Biol 129**:** 725-737.

Delattre, M., C. Canard and P. Gonczy, 2006 Sequential protein recruitment in C. elegans centriole formation. Curr Biol 16**:** 1844-1849.

Delattre, M., S. Leidel, K. Wani, K. Baumer, J. Bamat *et al.*, 2004 Centriolar SAS-5 is required for centrosome duplication in C. elegans. Nat Cell Biol 6**:** 656-664.

Fang, G., H. Yu and M. W. Kirschner, 1998 Direct binding of CDC20 protein family members activates the anaphase-promoting complex in mitosis and G1. Mol Cell 2**:** 163-171.

Fay, D. S., S. Keenan and M. Han, 2002 fzr-1 and lin-35/Rb function redundantly to control cell proliferation in C. elegans as revealed by a nonbiased synthetic screen. Genes Dev 16**:** 503-517.

Fu, J., I. M. Hagan and D. M. Glover, 2015 The centrosome and its duplication cycle. Cold Spring Harb Perspect Biol 7**:** a015800.

Ganem, N. J., S. A. Godinho and D. Pellman, 2009 A mechanism linking extra centrosomes to chromosomal instability. Nature 460**:** 278-282.

Garcia-Higuera, I., E. Manchado, P. Dubus, M. Canamero, J. Mendez *et al.*, 2008 Genomic stability and tumour suppression by the APC/C cofactor Cdh1. Nat Cell Biol 10**:** 802-811.

Glotzer, M., Murray, A.W., and M.W. Kirschner (1991). Cyclin is degraded by the ubiquitin pathway. Nature 349: 132-138.

Golden, A., P. L. Sadler, M. R. Wallenfang, J. M. Schumacher, D. R. Hamill *et al.*, 2000 Metaphase to anaphase (mat) transition-defective mutants in Caenorhabditis elegans. J Cell Biol 151**:** 1469-1482.

Gonczy, P., 2015 Centrosomes and cancer: revisiting a long-standing relationship. Nat Rev Cancer 15**:** 639-652.

Green, R. A., H. L. Kao, A. Audhya, S. Arur, J. R. Mayers *et al.*, 2011 A high-resolution C. elegans essential gene network based on phenotypic profiling of a complex tissue. Cell 145**:** 470-482.

Guderian, G., J. Westendorf, A. Uldschmid and E. A. Nigg, 2010 Plk4 trans-autophosphorylation regulates centriole number by controlling betaTrCP-mediated degradation. J Cell Sci 123**:** 2163-2169.

Habedanck, R., Y. D. Stierhof, C. J. Wilkinson and E. A. Nigg, 2005 The Polo kinase Plk4 functions in centriole duplication. Nat Cell Biol 7**:** 1140-1146.

Hartwell, L. H., and D. Smith, 1985 Altered fidelity of mitotic chromosome transmission in cell cycle mutants of S. cerevisiae. Genetics 110**:** 381-395.

Holland, A. J., W. Lan, S. Niessen, H. Hoover and D. W. Cleveland, 2010 Polo-like kinase 4 kinase activity limits centrosome overduplication by autoregulating its own stability. J Cell Biol 188**:** 191-198.

Irniger, S., and K. Nasmyth, 1997 The anaphase-promoting complex is required in G1 arrested yeast cells to inhibit B-type cyclin accumulation and to prevent uncontrolled entry into S-phase. J Cell Sci 110 (Pt 13)**:** 1523-1531.

Kemp, C. A., K. R. Kopish, P. Zipperlen, J. Ahringer and K. F. O'Connell, 2004 Centrosome maturation and duplication in C. elegans require the coiled-coil protein SPD-2. Dev Cell 6**:** 511-523.

Kemp, C. A., M. H. Song, M. K. Addepalli, G. Hunter and K. O'Connell, 2007 Suppressors of zyg-1 define regulators of centrosome duplication and nuclear association in Caenorhabditis elegans. Genetics 176**:** 95-113.

Kirkham, M., T. Muller-Reichert, K. Oegema, S. Grill and A. A. Hyman, 2003 SAS-4 is a C. elegans centriolar protein that controls centrosome size. Cell 112**:** 575-587.

Kitagawa, R., E. Law, L. Tang and A. M. Rose, 2002 The Cdc20 homolog, FZY-1, and its interacting protein, IFY-1, are required for proper chromosome segregation in Caenorhabditis elegans. Curr Biol 12**:** 2118-2123.

Kleylein-Sohn, J., J. Westendorf, M. Le Clech, R. Habedanck, Y. D. Stierhof *et al.*, 2007 Plk4-induced centriole biogenesis in human cells. Dev Cell 13**:** 190-202.

Kops, G. J., M. van der Voet, M. S. Manak, M. H. van Osch, S. M. Naini *et al.*, 2010 APC16 is a conserved subunit of the anaphase-promoting complex/cyclosome. J Cell Sci 123**:** 1623-1633.

Kraft, C., H. C. Vodermaier, S. Maurer-Stroh, F. Eisenhaber and J. M. Peters, 2005 The WD40 propeller domain of Cdh1 functions as a destruction box receptor for APC/C substrates. Mol Cell 18**:** 543-553.

Kumar, A., S. C. Girimaji, M. R. Duvvari and S. H. Blanton, 2009 Mutations in STIL, encoding a pericentriolar and centrosomal protein, cause primary microcephaly. Am J Hum Genet 84**:** 286-290.

Leidel, S., M. Delattre, L. Cerutti, K. Baumer and P. Gonczy, 2005 SAS-6 defines a protein family required for centrosome duplication in C. elegans and in human cells. Nat Cell Biol 7**:** 115-125.

Leidel, S., and P. Gonczy, 2003 SAS-4 is essential for centrosome duplication in C elegans and is recruited to daughter centrioles once per cell cycle. Dev Cell 4**:** 431-439.

Levine, M. S., B. Bakker, B. Boeckx, J. Moyett, J. Lu *et al.*, 2017 Centrosome Amplification Is Sufficient to Promote Spontaneous Tumorigenesis in Mammals. Dev Cell 40**:** 313-322 e315.

Livneh, I., V. Cohen-Kaplan, C. Cohen-Rosenzweig, N. Avni and A. Ciechanover, 2016 The life cycle of the 26S proteasome: from birth, through regulation and function, and onto its death. Cell Res 26**:** 869-885.

Medley, J. C., M. M. Kabara, M. D. Stubenvoll, L. E. DeMeyer and M. H. Song, 2017 Casein kinase II is required for proper cell division and acts as a negative regulator of centrosome duplication in Caenorhabditis elegans embryos. Biol Open 6**:** 17-28.

Meghini, F., T. Martins, X. Tait, K. Fujimitsu, H. Yamano *et al.*, 2016 Targeting of Fzr/Cdh1 for timely activation of the APC/C at the centrosome during mitotic exit. Nat Commun 7**:** 12607.

Miller, J. G., Y. Liu, C. W. Williams, H. E. Smith and K. F. O'Connell, 2016 The E2F-DP1 Transcription Factor Complex Regulates Centriole Duplication in Caenorhabditis elegans. G3 (Bethesda) 6**:** 709-720.

Nigg, E. A., and T. Stearns, 2011 The centrosome cycle: Centriole biogenesis, duplication and inherent asymmetries. Nat Cell Biol 13**:** 1154-1160.

O'Connell, K. F., C. Caron, K. R. Kopish, D. D. Hurd, K. J. Kemphues *et al.*, 2001 The C. elegans zyg-1 gene encodes a regulator of centrosome duplication with distinct maternal and paternal roles in the embryo. Cell 105**:** 547-558.

Paix, A., A. Folkmann, D. Rasoloson and G. Seydoux, 2015 High Efficiency, Homology-Directed Genome Editing in Caenorhabditis elegans Using CRISPR-Cas9 Ribonucleoprotein Complexes. Genetics 201: 47-54.

Pelletier, L., E. O'Toole, A. Schwager, A. A. Hyman and T. Muller-Reichert, 2006 Centriole assembly in Caenorhabditis elegans. Nature 444: 619-623.

Pelletier, L., N. Ozlu, E. Hannak, C. Cowan, B. Habermann *et al.*, 2004 The Caenorhabditis elegans centrosomal protein SPD-2 is required for both pericentriolar material recruitment and centriole duplication. Curr Biol 14: 863-873.

Peters, J. M., 2006 The anaphase promoting complex/cyclosome: a machine designed to destroy. Nat Rev Mol Cell Biol 7: 644-656.

Pfleger, C. M., and M. W. Kirschner, 2000 The KEN box: an APC recognition signal distinct from the D box targeted by Cdh1. Genes Dev 14: 655-665.

Praitis, V., E. Casey, D. Collar and J. Austin, 2001 Creation of low-copy integrated transgenic lines in Caenorhabditis elegans. Genetics 157: 1217-1226.

Prinz, S., E. S. Hwang, R. Visintin and A. Amon, 1998 The regulation of Cdc20 proteolysis reveals a role for APC components Cdc23 and Cdc27 during S phase and early mitosis. Curr Biol 8: 750-760.

Raff, J. W., K. Jeffers and J. Y. Huang, 2002 The roles of Fzy/Cdc20 and Fzr/Cdh1 in regulating the destruction of cyclin B in space and time. J Cell Biol 157: 1139-1149.

Rogers, G. C., N. M. Rusan, D. M. Roberts, M. Peifer and S. L. Rogers, 2009 The SCF Slimb ubiquitin ligase regulates Plk4/Sak levels to block centriole reduplication. J Cell Biol 184: 225-239.

Sarov, M., J. I. Murray, K. Schanze, A. Pozniakovski, W. Niu *et al.*, 2012 A genome-scale resource for in vivo tag-based protein function exploration in C. elegans. Cell 150: 855-866.

Schwab, M., A. S. Lutum and W. Seufert, 1997 Yeast Hct1 is a regulator of Clb2 cyclin proteolysis. Cell 90: 683-693.

Schwab, M., M. Neutzner, D. Mocker and W. Seufert, 2001 Yeast Hct1 recognizes the mitotic cyclin Clb2 and other substrates of the ubiquitin ligase APC. EMBO J 20: 5165-5175.

Shakes, D. C., A. K. Allen, K. M. Albert and A. Golden, 2011 emb-1 encodes the APC16 subunit of the Caenorhabditis elegans anaphase-promoting complex. Genetics 189**:** 549-560.

Shirayama, M., W. Zachariae, R. Ciosk and K. Nasmyth, 1998 The Polo-like kinase Cdc5p and the WD-repeat protein Cdc20p/fizzy are regulators and substrates of the anaphase promoting complex in Saccharomyces cerevisiae. EMBO J 17**:** 1336-1349.

Sigrist, S. J., and C. F. Lehner, 1997 Drosophila fizzy-related down-regulates mitotic cyclins and is required for cell proliferation arrest and entry into endocycles. Cell 90**:** 671-681.

Song, L., and M. Rape, 2008 Reverse the curse--the role of deubiquitination in cell cycle control. Curr Opin Cell Biol 20**:** 156-163.

Song, M. H., L. Aravind, T. Muller-Reichert and K. F. O'Connell, 2008 The conserved protein SZY-20 opposes the Plk4-related kinase ZYG-1 to limit centrosome size. Dev Cell 15**:** 901-912.

Song, M. H., Y. Liu, D. E. Anderson, W. J. Jahng and K. F. O'Connell, 2011 Protein phosphatase 2A-SUR-6/B55 regulates centriole duplication in C. elegans by controlling the levels of centriole assembly factors. Dev Cell 20**:** 563-571.

Strnad, P., S. Leidel, T. Vinogradova, U. Euteneuer, A. Khodjakov *et al.*, 2007 Regulated HsSAS-6 levels ensure formation of a single procentriole per centriole during the centrosome duplication cycle. Dev Cell 13**:** 203-213.

Stubenvoll, M. D., J. C. Medley, M. Irwin and M. H. Song, 2016 ATX-2, the C. elegans Ortholog of Human Ataxin-2, Regulates Centrosome Size and Microtubule Dynamics. PLoS Genet 12**:** e1006370.

Tang, C. J., R. H. Fu, K. S. Wu, W. B. Hsu and T. K. Tang, 2009 CPAP is a cell-cycle regulated protein that controls centriole length. Nat Cell Biol 11**:** 825-831.

Tang, C. J., S. Y. Lin, W. B. Hsu, Y. N. Lin, C. T. Wu *et al.*, 2011 The human microcephaly protein STIL interacts with CPAP and is required for procentriole formation. EMBO J 30**:** 4790-4804.

The, I., S. Ruijtenberg, B. P. Bouchet, A. Cristobal, M. B. Prinsen *et al.*, 2015 Rb and FZR1/Cdh1 determine CDK4/6-cyclin D requirement in C. elegans and human cancer cells. Nat Commun 6**:** 5906.

Thornton, B. R., T. M. Ng, M. E. Matyskiela, C. W. Carroll, D. O. Morgan *et al.*, 2006 An architectural map of the anaphase-promoting complex. Genes Dev 20**:** 449-460.

Visintin, R., S. Prinz and A. Amon, 1997 CDC20 and CDH1: a family of substrate-specific activators of APC-dependent proteolysis. Science 278**:** 460-463.

Zhang, S., L. Chang, C. Alfieri, Z. Zhang, J. Yang *et al.*, 2016 Molecular mechanism of APC/C activation by mitotic phosphorylation. Nature 533**:** 260-264.

Zhou, Y., Y. P. Ching, R. W. Ng and D. Y. Jin, 2003 Differential expression, localization and activity of two alternatively spliced isoforms of human APC regulator CDH1. Biochem J 374**:** 349-358.

Zhu, F., S. Lawo, A. Bird, D. Pinchev, A. Ralph *et al.*, 2008 The mammalian SPD-2 ortholog Cep192 regulates centrosome biogenesis. Curr Biol 18**:** 136-141.

Table 1. Genetic Analysis

	°C	% Embryonic Viability (Average ± SD)	n (progeny)
N2	24	99.4 ± 0.7	1500
zyg-1(it25)		0 ± 7.2	1350
fzr-1(bs31)		96.8 ± 5.0	1200
zyg-1(it25);fzr-1(bs31)		44.5 ± 7.3	1273
zyg-1(it25);fzr-1(bs38)		28.6 ± 10.3	1004
zyg-1(it25); M9 buffer		0 ± 0	600
zyg-1(it25); fzr-1(RNAi)		10.7 ± 7.9	1045
zyg-1(or409); M9 buffer		0 ± 0	466
zyg-1(or409); fzr-1(RNAi)		2.2 ± 0	313
N2	24	100 ± 0	1143
sas-5$^{KEN\text{-}to\text{-}3A}$		99 ± 1.1	1386
zyg-1(it25); sas-5$^{KEN\text{-}to\text{-}KEN}$		0 ± 0	1165
zyg-1(it25); sas-5$^{KEN\text{-}to\text{-}3A}$		0 ± 0	1216
N2	24	100 ± 0	437
zyg-1(it25)		0 ± 0	1573
mat-3(or180)		0 ± 0	636
zyg-1(it25); mat-3(or180)		5.1 ± 1.2	1300
N2	24	100 ± 0	437
zyg-1(it25)		4.0 ± 5.4	1159
emb-1(hc57)		3.2 ± 2.1	1064
zyg-1(it25); emb-1(hc57)		3.3 ± 4.3	1337
zyg-1(it25); sas-5$^{KEN\text{-}to\text{-}KEN}$	22.5	4.6 ± 4.0	1409
zyg-1(it25); sas-5$^{KEN\text{-}to\text{-}3A}$		35.3 ± 9.2	1341

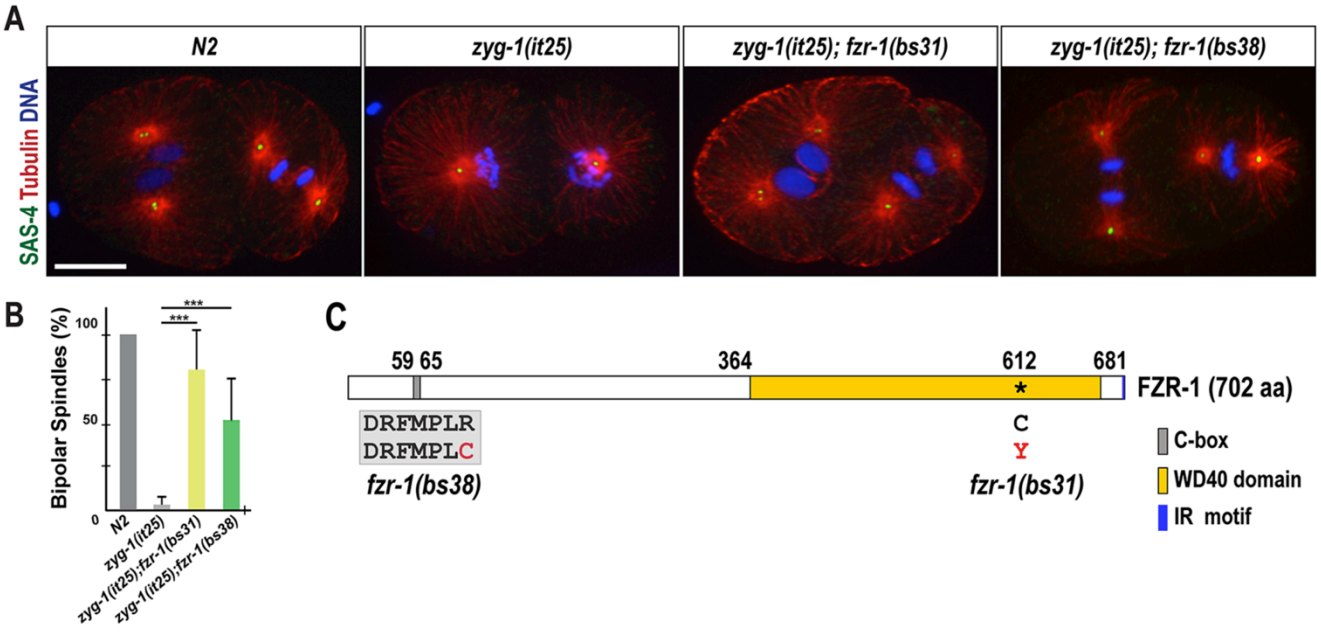

Figure 1. *fzr-1* mutations restore bipolar spindle formation to *zyg-1(it25)*. (A) Embryos grown at 24° stained for centrosomes (SAS-4), microtubules and DNA, illustrating mitotic spindles at the second mitosis. In *zyg-1(it25); fzr-1(bs31)* and *zyg-1(it25); fzr-1(bs38)* double mutant embryos, bipolar spindle formation is restored, whereas the *zyg-1(it25)* mutant embryo forms monopolar spindles. The *N2* embryo is shown as a wild-type control that shows bipolar spindles. Bar, 10 μm. (B) Quantification of bipolar spindle formation during the second cell cycle. At the restrictive temperature (24°), a great majority of *zyg-1(it25)* mutant embryos form monopolar spindles (3.3±4.4% bipolar spindles, n=660 blastomeres). In contrast, bipolar spindle formation is restored in *zyg-1(it25); fzr-1(bs31)* (79.9±22.0% bipolar spindles, n=276 blastomeres, $p<0.001$) and *zyg-1(it25); fzr-1(bs38)* (51.4±24.4% blastomeres, n=404 blastomeres, $p<0.001$) double mutants. Wild-type (*N2)* embryos invariably assemble bipolar spindles (100% bipolar spindles, n=600 blastomeres). Average values are presented. Error bars represent standard deviation (SD). (C) Schematic of FZR-1 protein structure illustrates functional domains and the location of the missense mutations: R65C within the C-box in the *fzr-1(bs38)* mutant, and C612Y within WD40 domain in the *fzr-1(bs31)* mutant allele.

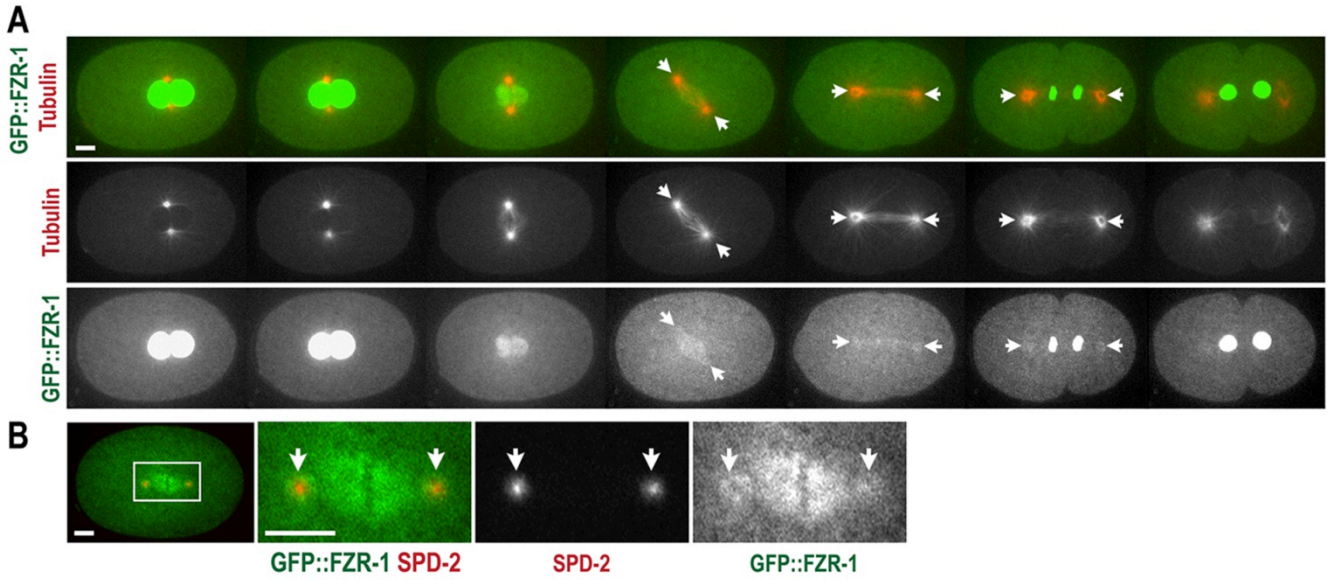

Figure 2. Subcellular localization of FZR-1 during the first cell cycle. (A) Still images from time-lapse movie of embryo expressing GFP::FZR-1 and mCherry::tubulin. Movie was acquired at 1 min interval. GFP::FZR-1 localizes at nuclei, mitotic spindles and centrosomes (arrows). Expression of mCherry::tubulin used as a subcellular land-marker. (B) Embryo expressing GFP::FZR-1 and mCherry::SPD-2 displays that GFP::FZR-1 localizes to mitotic spindles and centrosomes (arrows) that co-localize with mCherry-SPD-2, a centrosome marker. Bar, 5 μm.

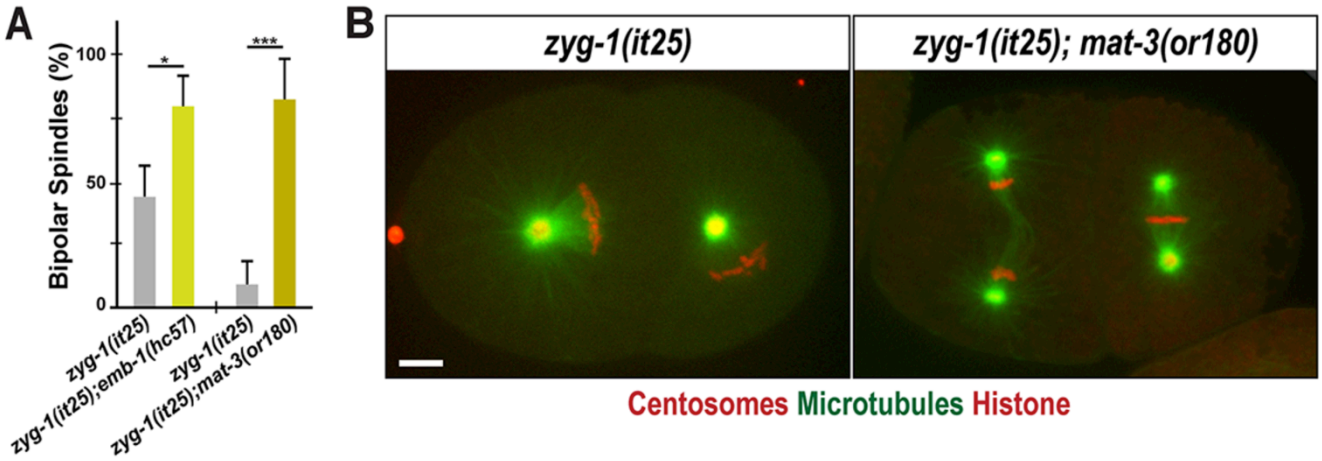

Figure 3. Inactivating the APC/C restores bipolar spindle formation to *zyg-1(it25)*. (A) Quantification of bipolar spindle formation during the second cell cycle. At 22.5°, there is an increase in bipolar spindle formation in *zyg-1(it25); emb-1(hc57)* double mutants (79.1±12.4%, n=228, *p*=0.03), compared to *zyg-1(it25)* single mutants (45.5±11.9%, n=238). At 24°, *zyg-1(it25); mat-3(or180)* double mutants assembled bipolar spindles at a significantly higher percentage (81.8±14.3%, n=78, *p*<0.001) than *zyg-1(it25)* embryos (9.1±8.8%, n=144). n is the number of blastomeres. (B) Still images of embryos expressing GFP::β-tubulin, mCherry::γ-tubulin (centrosome marker) and mCherry::histone raised at 24° illustrate monopolar spindle formation in the *zyg-1(it25)* embryo, and bipolar spindle formation in the *zyg-1(it25); mat-3(or180)* double mutant embryo. Bar, 5 μm.

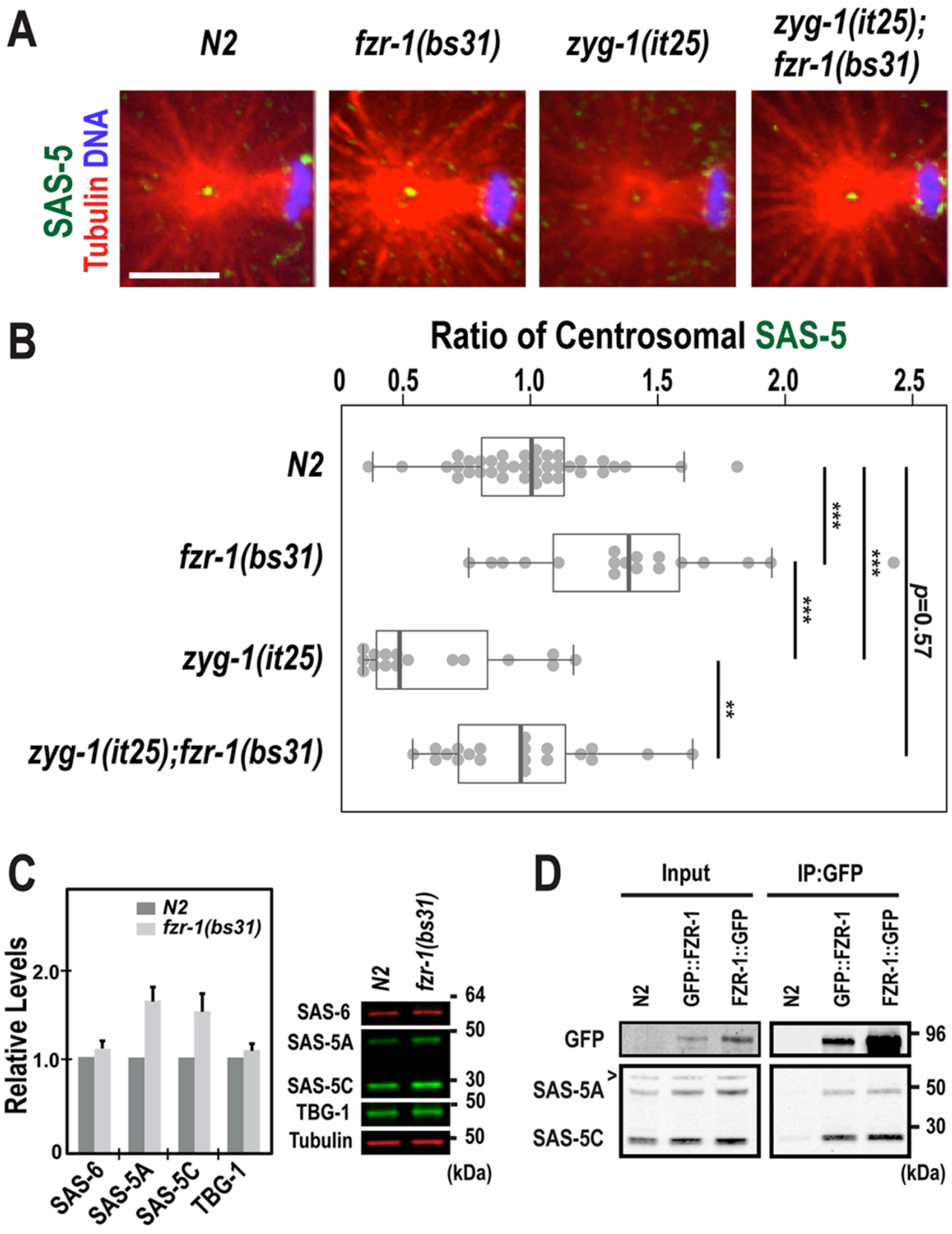

Figure 4. Loss of FZR-1 results in elevated SAS-5 levels. (A) Images of centrosomes stained for SAS-5 (green) at the first anaphase. Bar, 5 μm. (B) Quantification of centrosome-associated SAS-5 levels at the first

anaphase. SAS-5 levels are normalized to the average fluorescence intensity in wild-type centrosomes. *fzr-1(bs31)* embryos exhibit increased levels of centrosomal SAS-5 (1.41±0.42 fold, n=18; $p<0.001$) relative to wild-type embryos (1.00±0.28 fold, n=38). In *zyg-1(it25); fzr-1(bs31)* double mutants, centrosomal SAS-5 levels are restored to near wild-type levels (0.95±0.44 fold, n=20; $p=0.003$), compared to *zyg-1(it25)* embryos that show decreased levels of centrosomal SAS-5 (0.64±0.28 fold, n=16). n is the number of centrosomes. Each dot represents a centrosome. Box ranges from the first through third quartile of the data. Thick bar indicates the median. Dashed line extends 1.5 times the inter-quartile range or to the minimum and maximum data point. $^{**}p<0.01$, $^{***}p<0.001$ (two-tailed t-test). (C) Quantitative western blot analyses show that (left panel) *fzr-1(bs31)* mutant embryos possess increased levels of both SAS-5 isoforms, SAS-5A (1.56±0.16 fold) and SAS-5C (1.48±0.19 fold), compared to wild-type (*N2*) embryos. However, there were no significant differences in levels of either SAS-6 (1.09±0.08 fold) or TBG-1 (1.08±0.07 fold) between *fzr-1(bs31)* mutant and wild-type embryos. Four biological samples and eight technical replicates were used. Average values are presented and error bars are SD. (right panel) Representative western blot using embryonic lysates from *fzr-1(bs31)* mutants and *N2* animals. Tubulin was used as a loading control. (D) Immunoprecipitation (IP) using anti-GFP suggests that FZR-1 physically interacts with SAS-5. Both SAS-5 isoforms (SAS-5A, SAS-5C) co-precipitate with GFP::FZR-1 or FZR-1::GFP. Wild-type (*N2*) embryos were used as a negative control of IP. ~1% of total embryonic lysates was loaded in the input lanes. '>' indicates a non-specific detection by the SAS-5 antibody.

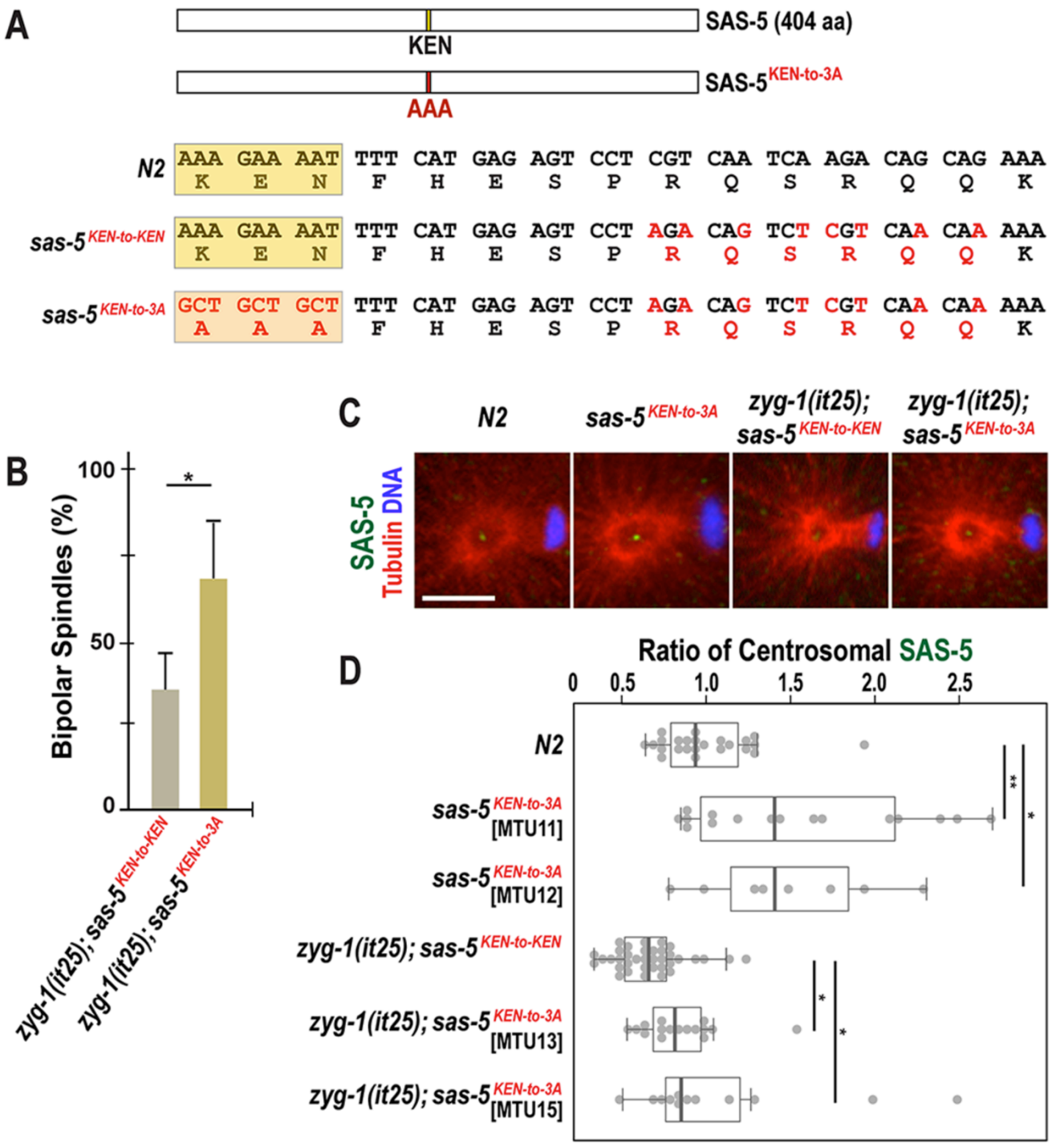

Figure 5. Mutation of the SAS-5 KEN-box leads to increased SAS-5 levels at centrosomes and restores centrosome duplication to *zyg-1(it25)* mutants. (A) SAS-5 contains a KEN-box (aa 213-216) motif. Mutations (red) are introduced at multiple sites to make alanine substitutions (AAA; 3A) for the KEN-box and additional silent mutations for the CRISPR genome editing (see methods and materials). The KEN-box is highlighted in yellow. Note that the *sas-5*$^{KEN\text{-}to\text{-}KEN}$ mutation contains the wild-type SAS-5 protein. (B) Quantification of bipolar spindle formation during the second cell cycle in *zyg-1(it25); sas-5*$^{KEN\text{-}to\text{-}KEN}$ and *zyg-1(it25); sas-5*$^{KEN\text{-}to\text{-}}$

^{3A} embryos at 22.5°. *zyg-1(it25); sas-5*$^{KEN\text{-}to\text{-}3A}$ double mutant embryos produce bipolar spindles at a higher rate (67.5±16.3%, n=124, *p*=0.02) than *zyg-1(it25); sas-5*$^{KEN\text{-}to\text{-}KEN}$ controls (35.1±10.7%, n=164). n is the number of blastomeres. Average values are presented and error bars are SD. (C) Centrosomes stained for SAS-5 (green) during the first anaphase. Bar, 5 μm. (D) Quantification of centrosomal SAS-5 levels during the first anaphase. We used two independently generated *sas-5*$^{KEN\text{-}to\text{-}3A}$ mutant lines to quantify SAS-5 levels (MTU11 and 12, Table S1). SAS-5 levels at centrosomes are normalized to the average fluorescence intensity in wild-type centrosmes. Mutating the SAS-5 KEN-box leads to increased levels of centrosomal SAS-5 in both MTU11 (1.54±0.63 fold, n=16; *p*=0.04) and MTU12 (1.48±0.50 fold, n=8; *p*=0.03), compared to wild type (1.00±0.29 fold; n=24 centrosomes). Consistently, there are a significant increase in centrosomal SAS-5 levels in both *zyg-1(it25); sas-5*$^{KEN\text{-}to\text{-}3A}$ double mutant lines (MTU13: 0.85±0.24 fold, n=16; *p*=0.01 and MTU15: 1.09±0.59 fold; n=12; *p*=0.03), compared to *zyg-1(it25); sas-5*$^{KEN\text{-}to\text{-}KEN}$ control that contains reduced levels of centrosomal SAS-5 (0.67±0.20 fold; n=36 centrosomes). n is the number of centrosomes. Each dot represents a centrosome. Box ranges from the first through third quartile of the data. Thick bar indicates the median. Dashed line extends 1.5 times the inter-quartile range or to the minimum and maximum data point. **p*<0.05, ***p*<0.01, ****p*<0.001 (two-tailed t-test).